

Effect of annealing on EPR spectra of Ti-Si-C-N samples*

N. GUSKOS^{1,2†}, E. A. ANAGNOSTAKIS³, G. ZOLNIERKIEWICZ², J. TYPEK², A. BIEDUNKIEWICZ⁴,
A. GUSKOS⁴, P. BERCZYNSKI²

¹Department of Solid State Physics, School of Physics, Faculty of Sciences, University of Athens,
Panepistimiopolis, 15 784 Zografos, Athens, Greece

²Institute of Physics, West Pomeranian University of Technology, Al. Piastow 48, 70-311 Szczecin, Poland

³Hellenic Air Force Academy; Dekeleia, Greece

⁴Institute of Materials Science and Engineering, West Pomeranian University of Technology,
Al. Piastow 19, 70-310 Szczecin, Poland.

Two nanocrystalline samples of TiC+SiC+20%C (sample 1) and Si₃N₄+Si(C,N)+Ti(C,N)+1%C (sample 2) were prepared by non-hydrolytic sol-gel method. The latter sample was produced from sample 1, by subjecting it to additional annealing at high temperature. XRD measurements showed the presence of aggregates of cubic SiC+TiC nanoparticles (10 to 30 nm in size). In both samples, a very narrow electron paramagnetic resonance (EPR) line originating from localized magnetic centers was centered at $g_{\text{eff}} \sim 2$. At $T = 130$ K, we registered the linewidths $\Delta H_{pp} = 1.41(2)$ G and $\Delta H_{pp} = 2.92(2)$ G for the sample without and with thermal annealing, respectively. For the non-annealed sample, the resonance line was fitted by a Lorentzian line in the low temperature range, and by a Dysonian line above 70 K, which indicates a significant change in electrical conductivity. Therefore, thermal annealing can significantly improve the transport properties of samples. An analysis of the temperature dependence of the EPR parameters (g -factor, linewidth, integrated intensity) showed that thermal annealing has a significant impact on the reorientation processes of localized magnetic centers.

Keywords: TiC, EPR, magnetic properties

© Wrocław University of Technology.

1. Introduction

Recently, Ti-Si-C-N compounds have been widely investigated, since the understanding of their physical properties can extend their application range [1–6]. One of the binary phases is titanium carbide (TiC) with electron type of conductivity, a superconducting state at low temperatures, high hardness (comparable to diamond), low thermal conductivity, and one of the highest melting points [7–14]. Additionally, titanium carbide is a structurally disordered system that can form many different sublattices [15], as well as phases in which ferromagnetic and superconducting states can coexist [16].

Electron paramagnetic resonance (EPR) of Ti-S-C materials indicated the presence of various localized magnetic centers producing very narrow and broad resonance lines [17–20]. The broad line originates from the complex of trivalent titanium ions, whereas the narrow line can be attributed to the conduction electrons or localized defects resulting in a Lorentzian or Dysonian lineshape (high conductivity is essential). These localized magnetic centers can significantly influence other physical properties of these materials. The reorientation of spins, strongly dependent on temperature, might play an important role with regard to the magnetic properties of these compounds. Also EPR is very useful in the study of aging processes. Many experiments point to the crucial role of annealing processes, the consequences of which can also be studied by EPR. Based on a large

*This paper was presented at the Conference Functional and Nanostructured Materials, FNMA 11, 6-9 September 2011, Szczecin, Poland

†E-mail: ngouskos@phys.uoa.gr

set of experimental data, the magnetic resonance could be an economical and sensitive method for characterizing Ti-Si-C materials. Recently, defective titanium oxide (TiO_2) has been widely studied [21–25]. Ferromagnetism discovered in undoped TiO_2 is related to oxygen vacancies (O_V), however, the mechanism remains unclear. Localized magnetic moments were detected after irradiation with 2 MeV oxygen ions, although the virgin sample was EPR silent down to low temperatures [25]. The EPR line was centered in the field corresponding to a g-value below 2. The electrons trapped by vacancies have g-values slightly larger than 2 and exhibit no hyperfine features [26, 27].

The aim of this report is to present the investigations of new nanocrystalline powder samples of $\text{TiC}+\text{SiC}+20\%C$ and $\text{Si}_3\text{N}_4+\text{Si}(\text{C},\text{N})+\text{Ti}(\text{C},\text{N})+1\%C$ using EPR in different temperature regions. The correlated spin reorientation processes can be responsible for the observed behavior of the EPR spectra in the low temperature regime.

2. Experimental

Nanocrystalline powder samples of $\text{TiC}+\text{SiC}+20\%C$ (sample 1) and $\text{Si}_3\text{N}_4+\text{Si}(\text{C},\text{N})+\text{Ti}(\text{C},\text{N})+1\%C$ (sample 2) were prepared using a non-hydrolytic sol-gel organotitanium precursor technique [28]. Sample 1 was prepared without additional thermal annealing, and after synthesis the powder was milled in a high-speed mill. Sample 2 was obtained by thermal annealing of sample 1 in an ultra-clean NH_3 atmosphere at 1623 K. During the annealing, the free carbon content decreased.

In order to characterize the samples, we performed X-ray diffraction (XRD) measurements by means of a copper X-ray tube ($\lambda = 1.5406\text{\AA}$) operating at a high voltage of 40 kV and at a current level of 40 mA. The average crystallite size was estimated according to the Scherrer formula $t = \frac{0.9\lambda}{B \cos \theta_B}$, where t is the average grain size, B is the width of the XRD peak at half intensity, λ is the X-ray wavelength, and θ_B is the peak angle.

The measurements of the temperature dependence of the EPR spectra of the samples containing ca. 20 mg of powder and placed in quartz tubes 4 mm in diameter, were obtained with a conventional X-band ($\nu = 9.4$ GHz) Bruker E 500 spectrometer with a 100-kHz magnetic field modulation. The measurements were carried out in the range from RT down to liquid helium with a stability of $\Delta T = \pm 1.0$ K by means of an Oxford cryogenic system.

3. Results and discussion

Fig. 1 presents the XRD patterns for sample 1 (without annealing) and sample 2 (with additional thermal annealing). The spectrum of sample 1 shows mainly the lines of TiC and SiC nanocrystallites covered with 20 % carbon of the average size of 15 nm. As a consequence of annealing (sample 2), the free carbon content decreased from 20 to below 1 wt.% and nanocrystallites of Ti(C,N) (regular system), Si(C,N) (trigonal system) smaller than 30 nm can be observed. Additionally, a very small amount of Si_3N_4 nanofibers is observed. A comparison of XRD patterns of the present samples with previously studied samples [20] reveal essential differences, particularly for the sample with additional thermal annealing. XRD peaks are weaker for sample 2 and the nanocrystalline Ti(C,N) peaks are more intense than those of Si(C,N), suggesting an increased concentration of this phase.

Fig. 2 shows SEM pictures of both samples. Before thermal annealing, larger aggregates of TiC and SiC exhibited nanosized granular structure (Fig. 2, panel a, sample 1). Sample 2 is composed of aggregates of cubic $\text{SiC}+\text{TiC}_x\text{N}_{1-x}$ nanoparticles with the addition of a small amount of Si_3N_4 nanofibers (Fig. 2b). The average diameter of a Si_3N_4 fibres is 50 nm (within a 10–90 nm range). The lengths of these fibres covers a wide range – from several nm up to a few μm . The size of granular $\text{SiC}+\text{TiC}_x\text{N}_{1-x}$ is smaller than previously observed, with a more complicated XRD pattern [19].

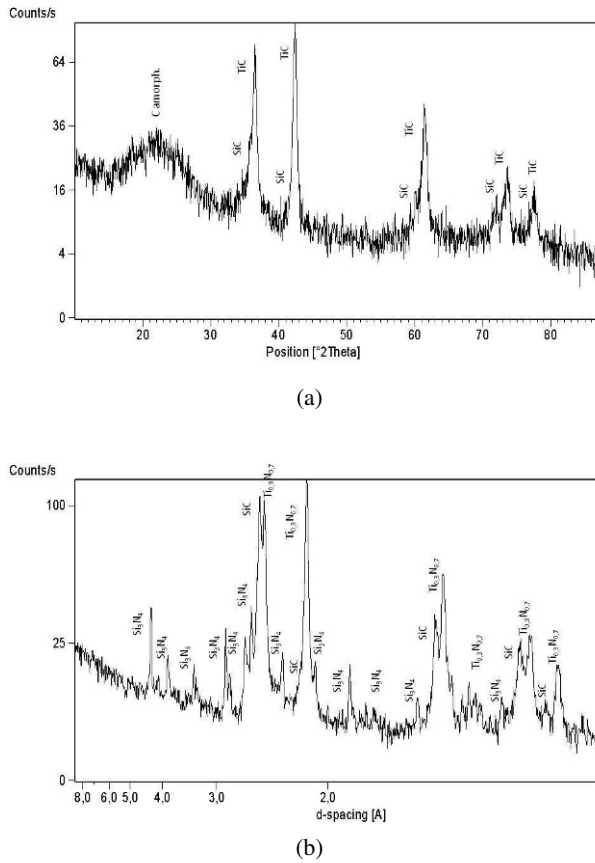
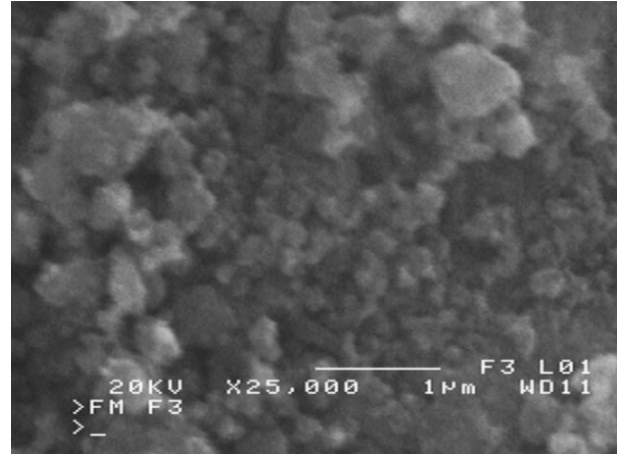
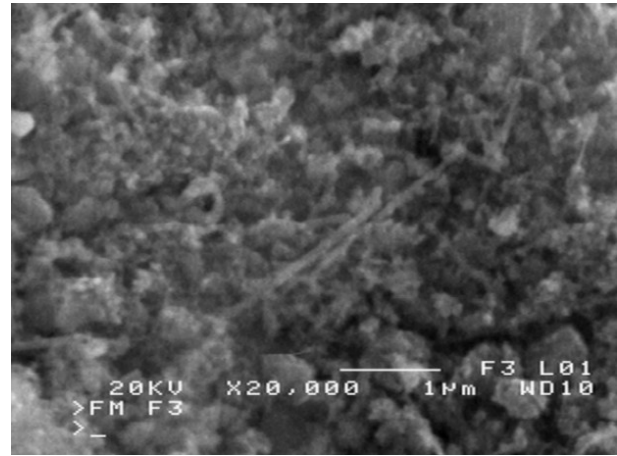


Fig. 1. XRD patterns of a) (TiC+SiC+20%C)(graphite) before annealing (sample 1), and b) ternary system $Si_3N_4+Si(C,N)+Ti(C,N)+1\%C$ obtained by annealing (sample 2).

Fig. 3 displays the EPR spectra of localized magnetic centers in samples 1 and 2, taken at different temperatures in the range of 3.7 – 290 K. In both samples, a very narrow EPR line originating from localized magnetic centers can be observed. At RT, a narrow line dominates the spectrum, centered at $g = 2.0036(2)$ with a peak-to-peak linewidth of $\Delta H_{pp} = 1.4(1)$ G and at $g = 2.0029$ with $\Delta H_{pp} = 1.7(1)$ G for samples 1 and 2, respectively. Since in both samples the line is asymmetric in the high temperature region, the best fit was obtained by using a Dysonian lineshape function. In contrast, an almost symmetric resonance line was recorded in the low temperature region for both samples and a good fit was obtained by using a Lorentzian



(a)



(b)

Fig. 2. SEM pictures of (a) sample 1, and (b) sample 2.

lineshape function. Fig. 4 presents the fitting of Lorentzian (left panels) and Dysonian (right panels) lines to experimental spectra (points) for sample 1 (upper panels) and sample 2 (lower panels). A Dysonian line is composed of absorption (A) and dispersion (D) terms:

$$\frac{d\chi}{dH} = A \frac{2x}{(1+x^2)^2} + D \frac{1-x^2}{(1+x^2)^2} \quad (1)$$

where $x = (H-H_r)/H_{pp}$, H_r is the resonance field and H_{pp} is the peak-to-peak linewidth. Often, the observed asymmetry of the line is expressed in terms of the ratio of the amplitude of the derivative absorption curve in high and low fields, termed the (A/B) ratio. This ratio is directly proportional

to the D/A ratio of Eq. 1. Fig. 5 presents the temperature dependence of the asymmetry ratio A/B in the high temperature range for sample 1. The asymmetry increases with an increase in temperature, indicating the increasing role of the conductivity of the sample.

Fig. 6 presents the temperature dependence of the calculated EPR parameters (resonance field, linewidth, integrated intensity) for both samples. Sample 2 exhibits a more intense EPR signal than sample 1 at RT, however, the opposite is observed in the low temperature region. Thermal annealing either played a significant role in the formation of additional paramagnetic centers or significantly changed the conducting properties of materials. The increase in the number of paramagnetic centers was estimated to be ca. 4 times larger for sample 2 at RT and 3 times larger for sample 1 at 9 K, as deduced from the ratio $A_1\Delta H_1^2/A_2\Delta H_2^2$, where $A_{EPR}(T)$ is the line peak-to-peak amplitude and ΔH_{pp} is the peak-to-peak linewidth. Indeed, due to thermal annealing, the amount of carbon decreased (from 20% to below 1%) in sample 2. The Dysonian lineshape of the resonance lines suggests the presence of appreciable electric conductivity in the samples, significantly larger in sample 1. The activation energy was smaller for sample 2, however, it leveled at lower temperatures for sample 1, in which the resonance line was well-described by the Lorentzian function. The ratio of $A_1\Delta H_1^2/A_2\Delta H_2^2$ for both samples decreased to 2.8 at 130 K and was significantly higher than for the samples studied in [20], where the integrated intensity was 1.7 times higher for the sample with thermal annealing. Sample 2 exhibited better conducting properties. For sample 2 at about 60 K, the linewidth changed drastically (Fig. 6, panel b). A similar change was observed for the annealed sample studied in [19], however, the temperature there was different (40 K). That difference can be associated with different conducting properties of these samples.

Significant changes in all studied EPR parameters at specific temperatures were recorded (Fig. 6). The position of the resonance line is shifted towards low magnetic fields with a decrease

in temperature (Fig. 6, panel a). The position of the line for sample 2 can be found at a slightly higher magnetic field than for sample 1 only up to 20 K (Fig. 6, panel a). A similar behavior was observed for the previously studied samples [20]. In the temperature range of 30–60 K, the resonance field was practically constant for sample 1, whereas slight changes were observed for sample 2, as in a previous study [20]. This suggests that in such a multiphase system, spin reorientation processes are more intense at low temperatures.

The rate of temperature change of the resonance field was $\Delta H_r/\Delta T \sim 4.8 \times 10^{-3}$ G/K (in the 290–55 K range) and $\Delta H_r/\Delta T \sim 26.8 \times 10^{-3}$ G/K (in the 50–4 K range) for sample 2, and $\Delta H_r/\Delta T \sim 7.3 \times 10^{-3}$ G/K (in the 290–80 K range) and $\Delta H_r/\Delta T \sim 263 \times 10^{-3}$ G/K (in the 20–3.3 K range) for sample 1. The above slope was larger for sample 1, both in the high and low temperature ranges. The shift of the resonance line resulted from the change in the resonance condition $h\nu = g\mu_B(H_o + H_{dip})$, where h is the Planck constant, ν is the resonance frequency, g -factor is the spectroscopic coefficient, μ_B is the Bohr magneton, H_o is the externally applied magnetic field, and H_{dip} is the internal magnetic field produced by the dipole-dipole interaction. The internal magnetic field was created by the correlated fluctuating spin system. In a disordered system, the competition between magnetic interactions in a spin system can have a significant influence on the behavior of the resonance line with changing temperature. Freezing processes can be responsible for the reorientation of spins, especially at low temperatures. The observed sharp change at about 60 K can be related to the transition between the conducting and isolating phase, particularly intense in sample 1. The slope $\Delta H_r/\Delta T$ changed by two orders of magnitude for sample 1 and by one order of magnitude for sample 2. The integrated intensity indicates that in the low temperature range the number of spins was smaller in sample 2. The freezing processes in the system of interacting spins with a low concentration of spins can be responsible for a decrease in the value of the aforementioned slope.

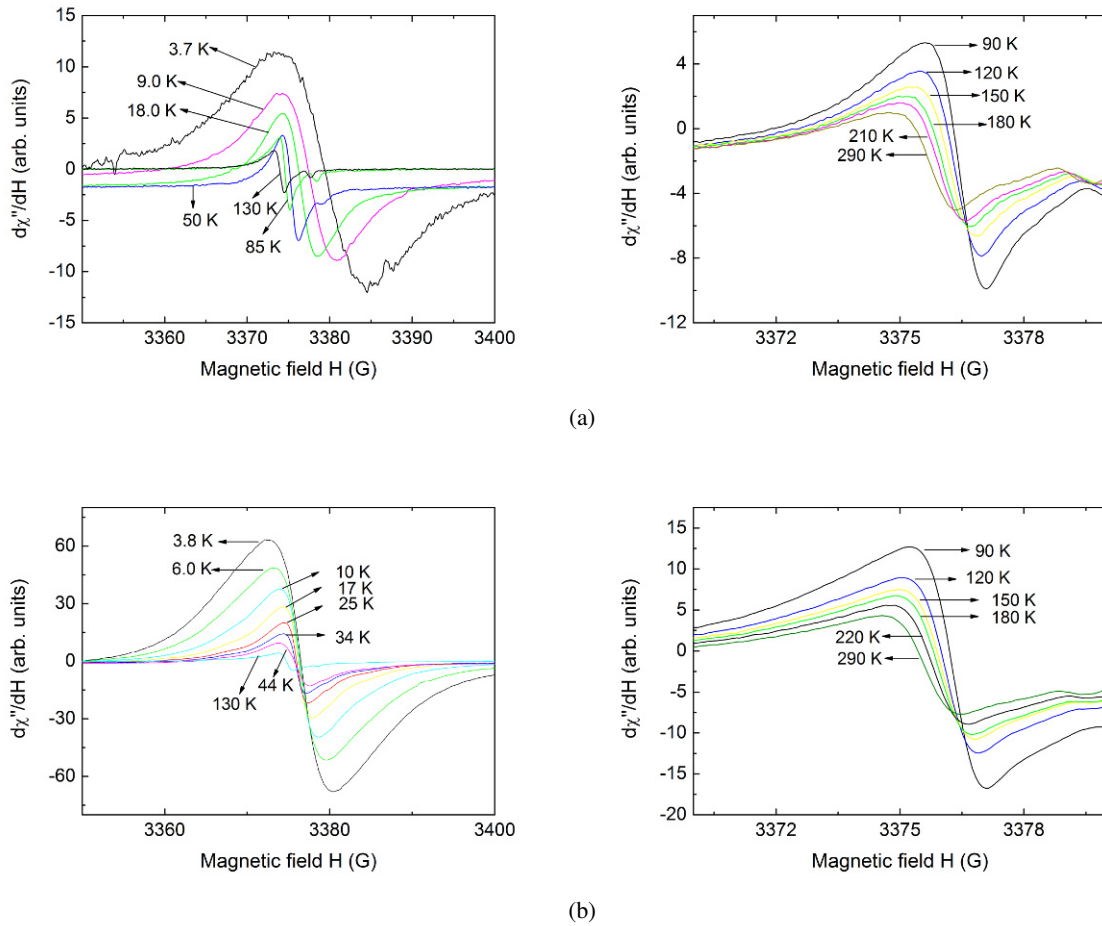


Fig. 3. EPR spectra of two Ti-Si-C-N samples, registered at different temperatures: (a) before annealing (sample 1) – in the low temperature range (left panel), in the high temperature range (right panel); (b) after annealing (sample 2) – in the low temperature range (left panel), in the high temperature range (right panel).

The linewidth of the resonance line increased with a decrease in temperature for both samples, however, the rate of this change was significant only in the low temperature range (see Fig. 6, panel b). To reveal the different temperature ranges of the relaxation processes responsible for the linewidth, a log-log plot of the linewidth ΔH_{pp} versus the shift of the resonance field $\delta H_r = H_r(T) - H_r(\infty)$ is presented in Fig. 7. $H_r(\infty)$ is the resonance field in the limit of very high temperatures. Any detected changes in the slope indicate a change in the type of relaxation in the samples. Fig. 5 reveals the existence of three temperature ranges. The limiting temperatures are 70 K and 33 K for sample 1, and 90 K and 20 K for sample 2,

separating the intermediate range from the high and low temperature ranges. A comparison of both samples shows that the high temperature range was wider for sample 1, in which the jump to the intermediate range was higher. Unlike in sample 1, the intermediate temperature range for sample 2 could be divided into two regions: 90–55 K and 55–20 K. Unexpected jumps observed at certain temperatures for the linewidth, g -factor and integrated intensity serve as a further evidence of a magnetically inhomogeneous state. The short-range magnetic order, confined to distinct spatial regions, can trigger a sharp variation in the EPR parameters and inhibit long-range magnetic order. Similar behavior was observed

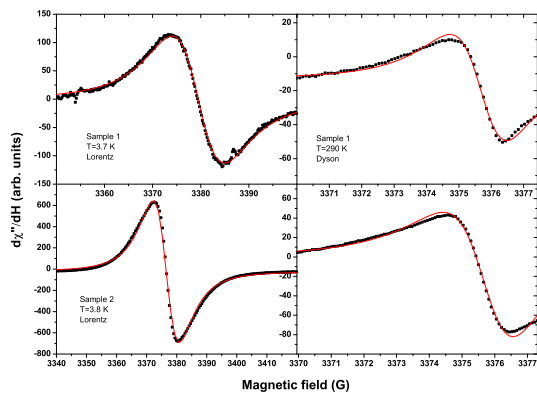


Fig. 4. Fitting of Lorentzian (left panels) and Dysonian (right panels) lines to the experimental spectra (points) for sample 1 (upper panels) and sample 2 (lower panels).

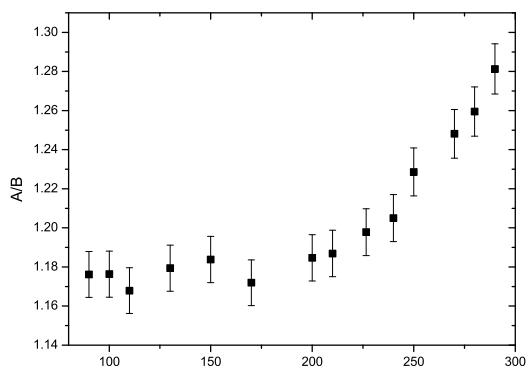


Fig. 5. Temperature dependence of the line asymmetry ratio A/B in the high temperature range for sample 1.

for paramagnetic centers in substantially different compounds (ternary vanadates) [29, 30].

Fig. 6, panel d presents the temperature dependence of the reciprocal of the integrated intensity. The EPR integrated intensity, defined as the area under the absorption resonance curve, is proportional to the imaginary part of the complex magnetic susceptibility. For both samples, three different regimes of the evolution of the Curie-Weiss temperature can

be recognized. The fitting of $I_{EPR}(T)$ to the Curie-Weiss law, $C/(T-\Theta)$, where C is the Curie constant and Θ is the Curie-Weiss temperature, indicates that in the high temperature range, a negative and very high Curie-Weiss temperature is present and takes up the following values: $\Theta(1)_{250-130} \sim -200$ K, $\Theta(1)_{130-45} \sim -130$ K for sample 1; and $\Theta(2)_{250-130} \sim -200$ K, $\Theta(2)_{130-45} \sim -330$ K for sample 2. In the low temperature range, the Curie-Weiss temperature is positive and rather small: $\Theta(1) < 10 \sim 2$ K for sample 1; and $\Theta(2) < 10 \sim 2.5$ K for sample 2. The negative value of the Curie-Weiss temperature indicates the presence of strong antiferromagnetic interactions, whereas a positive value of Θ indicates the presence of ferromagnetic interactions between localized magnetic centers. In previously investigated samples, significant ferromagnetic interactions were observed in the high temperature range [20]. The coupling of localized magnetic centers with conducting electrons could cause the strong antiferromagnetic interactions to dominate at high temperatures. The competition of magnetic interactions in different sublattices prevents the formation of long-range magnetic order at high temperatures [31, 32]. The presence of low-temperature ferromagnetic interactions was also detected in a similar material, a TiC_x/C nanocomposite [16]. Dc magnetization measurements revealed a strong ferromagnetic component at $T < 10$ K and a Curie-Weiss behavior at $T > 70$ K with a Curie-Weiss temperature $\Theta = -20$ K [16].

In order to explain the EPR results of our investigations, we propose to apply the model of two exchange-coupled systems of localized defects and conduction electrons in the bottleneck regime [33]. A comparison of the EPR effects of electron irradiation on carbon nanotubes and of thermal annealing on our sample shows remarkable similarities. The intensity of the EPR signal increased, whereas the linewidth and the g -factor decreased. Although two different spin systems were present in the investigated samples, there was only one EPR line, because the two systems were strongly exchange-coupled. The bottleneck

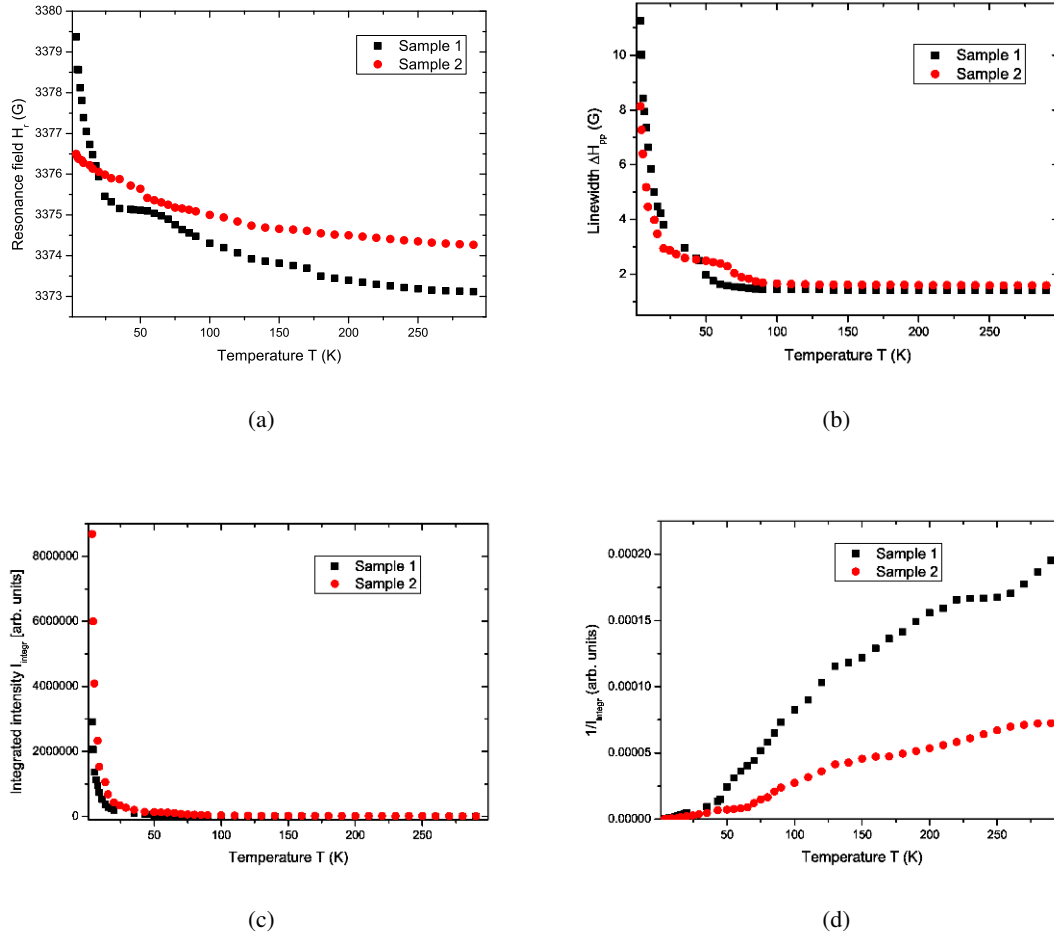


Fig. 6. Temperature dependence of the EPR parameters for both samples, before annealing (sample 1) and after annealing (sample 2): (a) resonance field; (b) linewidth; (c) integrated intensity; (d) reciprocal of the integrated intensity.

regime resulted in the prevalence of one of the spin systems in the overall behavior – the one with the dominating contribution to the magnetic susceptibility. Thus, the conduction-electron spins dominated at high temperatures, whereas the localized spins dominated at low temperatures.

The observed EPR signal cannot be attributed to the Ti^{3+} paramagnetic ions, since even in powdered crystalline (and nanocrystalline) compounds, the Ti^{3+} centers ($3d^1$ electronic configuration) are characterized by a strongly anisotropic g -factor in general axial symmetry. For example, in the $\text{Al}_3\text{Be}_3(\text{SiO}_3)_6$ crystal, the EPR spectrum

of the Ti^{3+} ions in octahedral coordination is characterized by the following g -factor values at $T = 77$ K: $g_{\parallel} = 1.9717$, $g_{\perp} = 1.8391$ [34]. In irradiated alkali titanate glasses, two types of anisotropic Ti^{3+} centers were observed: one was characterized by a broad line with $g_{\parallel} = 1.89$, and $g_{\perp} = 1.98$, whereas the other was related to a narrow line with $g_{\parallel} = 1.98$, $g_{\perp} = 1.99$ [35]. A possible explanation of the observed EPR spectrum involves electrons trapped by vacancies or defects, which is suggested by the fact that their g -factor was slightly larger than 2 and did not exhibit a hyperfine structure [26, 27].

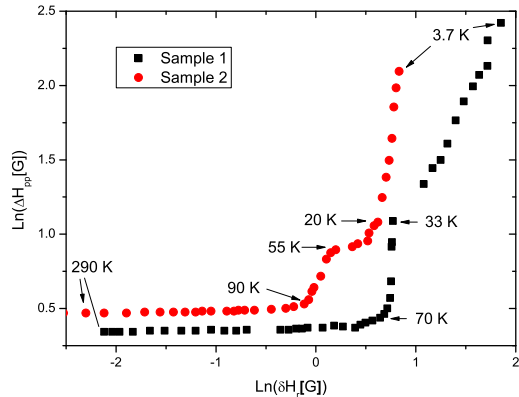


Fig. 7. Plot of $\ln(\Delta H_{pp})$ vs. $\ln(\delta H_r)$ for samples 1 and 2. Characteristic temperatures are indicated.

Even the presence of a very small amount of magnetic nanoparticles embedded in a nonmagnetic matrix could significantly improve the magnetic and mechanical properties of the matrix [36–40]. Strong antiferromagnetic interactions at high temperature provide additional attractive force in the investigated samples, which improves their mechanical properties. For sample 2 (subjected to thermal annealing), the value of the Curie-Weiss temperature is significantly higher and, thus, its potential applications are better. We believe that EPR is very useful for the characterization of such materials.

4. Conclusions

Small concentration of localized magnetic centers in disordered and multiphase Ti-Si-C-N systems is a very interesting subject for studying the reorientation of correlated spins and the observation of their temperature dependence. Strong antiferromagnetic interaction was observed at high temperatures, whereas the ferromagnetic interaction dominated at low temperatures. To explain the observed EPR thermal behavior of both samples, we proposed the model of two exchange-coupled systems of localized defects and conduction electrons in the bottleneck regime. We suggest that $\text{Ti}^{3+}\text{-O}_V$ defect complexes can be generated during thermal annealing following

the formation of trivalent titanium ions, which provide local $3d$ moments. These local magnetic moments can be involved in the observed ferromagnetism. In the high temperature range, the EPR spectra reflected the dominating role of conduction electrons, whereas in the low temperature range, the localized spins dominated. Strong antiferromagnetic interactions can improve the mechanical properties of the studied samples. Thus, thermal annealing can widen the range of possible applications of the investigated samples.

References

- [1] EKLUND P. et al., *Phys. Rev. B*, 74 (2006), 045417.
- [2] YONG E. Y., KIM Y. C., LEE S., KIM N., *J. Metal. Mater. Trans. A*, 35 (2007), 1029.
- [3] LEROY W. P., DETAVERNIER C., VAN MEIRHAEGHE R. L., LAVOIE C., *J. Appl. Phys.*, 101 (2007), 053714.
- [4] CORDOBA J. M., SAYAGUES M. J., ALCALA M. D., GOTOR F. J., *J. Am. Ceram. Soc.*, 90 (2007), 825.
- [5] ISAEV E. I. et al., *J. Appl. Phys.*, 101 (2007), 123519.
- [6] VALLAURI D., ATIAS CITYPLACEADRIAN I.C., CHRYSANTHOU A., *J. Eur. Ceram. Soc.*, 28 (2008), 1697.
- [7] TOTH L. E., *Transition Metal Carbide and Nitrides*, Academic Press, New York 1971.
- [8] REMPEL A. A., *Usp. Fiz. Nauk (Russia)*, 166 (1966), 33.
- [9] IZQUIERDO J., VEGA A., BOUARAB S., KHAN M. A., *Phys. Rev. B*, 58 (1998), 3507.
- [10] ACHA C. et al., *Eur. Phys. J. B*, 34 (2003), 421.
- [11] GUSKOS N. et al., *Rev. Adv. Mater. Sci.*, 8 (2004), 49.
- [12] GUSEV A. I., NAZAROVA S. Z., *Usp. Fiz. Nauk (Russia)*, 175 (2005) 682.
- [13] ISAEV E. I. et al., *Phys. Rev. B*, 72 (2005), 064515.
- [14] IVANOVSKII A. I., *Theor. Exp. Chem.*, 43 (2007), 1.
- [15] WILLIAMS W. S., *Prog. Solid State Ch.*, 6 (1971), 57.
- [16] GUSKOS N. et al., *J. Non-Cryst. Solids*, 354 (2008), 4330.
- [17] BODZIONY T. et al., *Mater. Sci.-Poland* 23 (2005), 899.
- [18] GUSKOS N., BODZIONY T., BIEDUNKIEWICZ A., AIDINIS C., *Acta Phys. Pol. A*, 108 (2005), 311.
- [19] GUSKOS N., BODZIONY T., MARYNIAK M., TYPEK J., BIEDUNKIEWICZ A., *J. Alloy. Compd.*, 455 (2008), 52.
- [20] GUSKOS N. et al., *Rev. Adv. Mater. Sci.*, 23 (2010), 189.
- [21] COEY J. M. D., VENKATESAN M., STAMENOV P., FITZGERALD V. C. B., DORNELES L. S., *Phys. Rev. B*, 72 (2005), 024450.
- [22] YOON S. D. et al., *J. Phys.: Condens. Matter*, 18 (2006), L355.
- [23] HONG N. SAKAI H., J., POIROT N., BRIZÉ V., *Phys. Rev. B*, 73 (2006), 132404.

- [24] ZHOU S. et al., *J. Phys. D*, 41 (2008), 105011.
- [25] ZHOU S. et al., *Phys. Rev. B*, 79 (2009), 113201.
- [26] STERRER M., FISCHBACH E., RISSE T., FREUND H.-J., *Phys. Rev. Lett.*, 94 (2005), 186101.
- [27] CHONG S. V., KADOWAKI K., XIA J., IDRIS H., *Appl. Phys. Lett.*, 92 (2008), 232502.
- [28] BIEDUNKIEWICZ A., STRZELCZAK A., MOZDZEN G., LELATKO J., *Acta Mater.*, 56 (2008), 3132.
- [29] GUSKOS N. et al., *J. Non-Cryst. Solids*, 352 (2006), 4179.
- [30] GUSKOS N. et al., *J. Appl. Phys.*, 101 (2007), 103922.
- [31] ZOLNIERKIEWICZ G., GUSKO N. TYPEK J., BLONSKA-TABERO A., *Acta Phys. Pol. A*, 109 (2006), 675.
- [32] ZOLNIERKIEWICZ G. et al., *J. Alloy. Compd.* 471 (2009), 28.
- [33] BEUNEU F., HUILLIER C., SALVETAT J. P., BONARD J. M., FORRO L., *Phys. Rev. B*, 59 (1999), 5945.
- [34] BERSHOV L. V., *Zh. Strukt. Khim.*, 10 (1969), 141.
- [35] KIM Y. M., BRAY P. J., *J. Chem. Phys.*, 53 (1970), 716.
- [36] GUSKOS N. et al., *Mater. Sci.-Poland*, 23 (2005), 972.
- [37] NARKIEWICZ U. et al., *Mater. Sci.-Poland*, 24 (2006), 1067.
- [38] BLYSZKO J. et al., *J. Non-Cryst. Solids*, 354 (2008), 4515.
- [39] MARYNIAK M. et al., *Polimery-W.*, 54 (2009), 546.
- [40] GUSKOS N. et al., *Rev. Adv. Mater. Sci.*, 23 (2010), 113.

Received 2012-01-07

Accepted 2012-05-01